DESIGN OF A NOVEL INTEGRATED POLARIZATION BEAM SPLITTER

Bogdan CĂLIN[1], Marian ZAMFIRESCU[2], Radu IONICIOIU[3], Niculae PUŞCAŞ[4]

We propose an integrated polarization beam splitter based on a two-dimensional photonic crystal of polymer cylinders in air, with a TE bandgap centered on a wavelength of λ=780nm. The novel design is tailored for two-photon absorption 3D laser direct writing in a polymeric photoresist. Using this fabrication method, we can obtain spatial features as small as 200 nm. Processing time can be as low as 15 minutes for a 300x300 µm processed area and an overall cost of ~15 eur. The device is comprised of a series of components such as linear waveguides, parabolic tapered waveguides and multimode interference couplers, in order to lower optical losses. In this paper, design steps and simulation results are presented and discussed. Experimental results supporting the chosen fabrication method and materials are presented and discussed in the form of a parametric study.

1. Introduction

Integrated polarization beam splitters (PBS) and photonic crystals represent complex optical microstructures with various applications. Photonic crystals may be used in fiber fabrication for more efficient light confinement [1] or as wavelength filters [2], due to the existence of photonic band gaps. Furthermore, these band gaps can manifest for specific polarizations of incident light, which not only extends the applications of photonic crystals as filters, but they can also be employed in complex optical structures that act as a PBS. [3], [4], [5]. There are various design approaches for a photonic crystal based PBS. One approach is using a photonic crystal as a filter to separate TE and TM modes guided with linear waveguides [3], [6] or even planar waveguides [4]. Such design

[1] PhD, Student, Doctoral School of the Faculty of Applied Physics, University POLITEHNICA of Bucharest, Romania; e-mail: bogdan.calin@physics.pub.ro ; and Laser Material Processing Laboratory, National Institute for Laser, Plasma and Radiation Physics – CETAL Dept., Bucharest-Măgurele, Romania;
[2] Laser Material Processing Laboratory, National Institute for Laser, Plasma and Radiation Physics – CETAL Dept., Bucharest-Măgurele, Romani
[3] Senior Researcher, Dept. of Theoretical Physics, Horia Hulubei National Institute for Physics and Nuclear Engineering, Bucharest-Măgurele, Romania
[4] Prof., Dept. of Physics, University POLITEHNICA of Bucharest, Romania

requires a large width waveguide at the contact with the crystal, to avoid large diffraction angles at the output of the linear waveguide (input of the polarizing crystal). Large diffraction angles determine a board transverse intensity distribution which affects the collecting of light after polarization splitting. Another approach is to integrate waveguides into the polarizing photonic crystal. Polarization splitting can be achieved using various methods. One method is constructing a photonic crystal directional coupler inside the crystal, and use the different coupling lengths of each propagation mode to separate them [5]. Another method is using hybrid photonic crystals [7]. By "hybrid", we refer to two photonic crystals with different geometries integrated in one structure. In this case, one photonic crystal possesses band gaps for both TE and TM modes, and is used to host linear waveguides for light guiding. The second photonic crystal is used as a filter and has high transmission for one of the propagation modes, while also possessing low transmission for the other.

The domain of integrated optics has undergone significant development over the years and is currently promoted by the recent advances in quantum computing and quantum key distribution [8]. Various fabrication methods and technologies have been successfully employed to obtain photonic crystals with two-dimensional geometry [9], [10], [11], different types of 3D geometries (wire [12], woodpile [13], stacked spheres [14], etc), and combinations between 2D and 3D [15]. Generally used methods are Direct Laser Writing (DLW) [16], lithography [10] and autocloning [2]. Although DLW is flexible and easy to implement, it has limited optical and spatial resolution. Two-photon polymerization (TPP) partially solves the resolution problem by processing samples under the diffraction limit. TPP-based direct laser writing (TPP-DLW) is shortly discussed along with experimental results. Lithographic methods offer best spatial features and reproducibility, but employing the method is more resource and time consuming in comparison to DLW. Autocloning is a special method used for fabrication of 3D photonic crystals that present band gaps in the visible spectrum, using appropriately-configured multilayer thin films.

In this paper, a complex photonic structure acting as a narrow-band polarization beam splitter for a wavelength of λ=780 nm is discussed. The core of the device consists of a two-dimensional photonic crystal with a TE band gap. In order to increase the optical power output, several complementary components are used. These components are parabolic and linear tapered waveguides and a multimode interference coupler (MMI). The device is presented in figure 1. We discuss a step-by-step methodology for the optimization of the photonic crystal. We also address device fabrication as the targeted method is the TPP – DLW, due to its potential for cheap and rapid prototyping of photonic structures. We present

and discuss experimental results regarding the feasibility of the proposed fabrication method.

2. Design and simulation of the PBS

The device was designed and simulated using the OptiFDTD package, a finite-difference time-domain (FDTD) based software package that allows the development of complex optical and plasmonic structures. The FDTD numerical method is simple to implement and offers good results. Main disadvantage of this method is that it requires larger computational resources compared to alternative methods (finite element method or beam propagation method). The device discussed in this paper is centered around a planar 2D photonic crystal with higher index cylinders in air. The schematic is presented in figure 1. The structure is made of IP-L on a SiO_2 substrate. IP-L is a liquid polymeric photoresist optimized for laser direct writing through two-photon absorption at sub-micron resolutions. Irradiation of this photoresist with near-IR femtosecond pulses triggers a photochemical reaction that results in chain polymerization. The refractive index of IP-L and SiO_2 are 1.48 and respectively 1.45 for a wavelength λ=780 nm.

The choice of material is motivated by the ease of fabrication through oil-immersed TPP-DLW. Solutions to Helmholtz equations can be treated separately for each of the 3 spatial axes. Simulations are two dimensional (Z direction is considered infinite). The device is intended as a planar optical device, and the height of the structure can be evaluated independently.

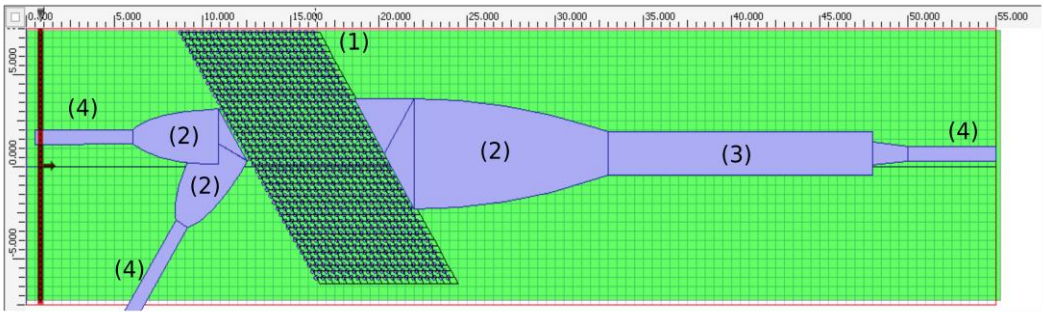

(1) Photonic Crystal
(2) Parabolic Tapered Waveguides
(3) Multimode Interference Coupler
(4) Linear Waveguides

Fig. 1: Schematic of the photonic crystal PBS.

2.1.**Photonic crystal design**

The core of the device is a photonic crystal with a hexagonal lattice with a parallelepiped fill of higher index cylinders in air. A hexagonal lattice has a better filling factor, resulting in larger photonic band gaps [17].

There are multiple approaches when designing a 2D photonic crystal. Some of the parameters are fixed by the intended fabrication method and material of choice (n=1.48, λ=780 nm, photonic atom is a cylinder in air, determined by the laser transverse intensity profile). Photonic crystals are fully scalable optical devices. By this we mean that its behavior is determined by the correlation of its geometry with the wavelength of the light propagating through it, and not by physical dimensions. In other words, photonic band structure scales linearly with crystal dimensions, as long as the fill factor is respected. The fill factor is defined as the total area of the photonic atom over the total area of the primitive cell (volume is used for 3D simulations). As an example, the design of the photonic crystal discussed in this paper started with a hexagonal lattice of cylinders in air. The cylinder diameter is half of the primitive cell vector (hexagonal lattice primitive cell is defined by two equal vectors). This starting point results in a filling factor of ~22.7 %.

Our approach for designing a slab 2D photonic crystal can be summarized as follows: we start with an arbitrary hexagonal lattice of cylinders in air, find the optimal fill factor, then scale the whole crystal to fit the target wavelength. In this case, we start from a lattice defined by vectors equal to 1 μm. The photonic atom is cylindrical and has a diameter of half of one of the vectors determining the primitive cell. We keep the refractive index of n=1.48 and λ=780 nm fixed, for reasons mentioned previously, and vary the geometrical parameters. We start by studying how the photonic band gaps vary with respect to cylinder diameter, and we modify the lattice itself only after determining the optimal fill factor.

In order to determine the largest band gap, the first step is to modify the photonic atom by incrementally increasing and decreasing its diameter until the band gap completely disappears. We calculate the band structure and get the width of the band gap for each diameter of the photonic atom. Plotting the band gap width as a function of cylinder diameter allows us to extrapolate the optimal diameter (and fill factor, implicitly) in order to obtain the maximum band gap. We then scale the photonic crystal in order to center the band gap on the desired wavelength. Simulations indicate that the IP-L cylinders in air crystal shows band gaps for TE modes and none for TM. This is contrary to the empirically determined tendency that 2D photonic crystals present band gaps the other way around [18] [19]: cylinders in air are associated with TM gaps, while air holes in a

slab waveguide are associated with TE gaps. Low refractive index contrast could be the determining factor for these results, but further investigations are required.

In figure 2, we plot the variation of the TE band gap with respect to cylinder diameter, for the final scale of the crystal (band gap centered on λ=780 nm). From figure 2, we chose the diameter of 220 nm of the photonic atoms, maximum the band gap. We determined the vectors of the primitive cell to be ~394 nm.

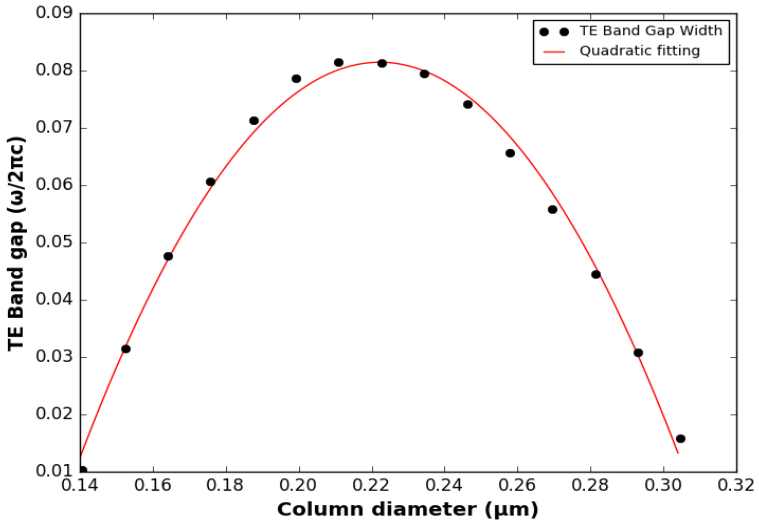

Fig. 2: Plot of TE Band gap as a function of IP-L cylinder diameter for a

The photonic band structure of the optimized crystal can be observed in figure 3. A complete band gap for the TE mode is present. The band gap is narrow due to low refractive index contrast, which determines the crystal to act as a narrow-band polarizer. A TM band gap is present as well for a specific propagation direction (“M” direction). In order to improve functionality of the device, the input propagation direction must be parallel to the “X” direction of the irreducible Brillouin zone (not to be confused with the X axis of the geometrical layout; see figure 3). This determines lower dispersion for light propagating in the Z direction (fig. 1). As presented in figure 1, input light propagates in the Z direction. Considering the input wavelength λ=780 nm, the photonic band structure indicates TE modes will be reflected while TM modes will be transmitted, as it was intended.

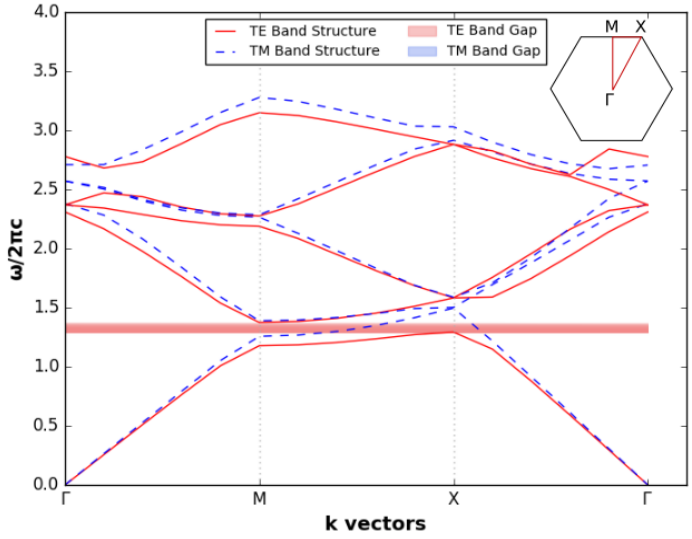

Fig. 3: Photonic band structure of the 2D hexagonal photonic crystal of IP-L cylinders in air, for both TE and TM polarizations.

2.2.Input and output coupling for the photonic crystal

Many photonic integrated circuits employ the use of single-mode waveguides for better control of the optical properties of input waves. A wide input intensity distribution is similar to the PBS design approach where the crystal acts only as a polarization filter [3], [6]. We propose a series of parabolic tapered waveguides and a multimode interference coupler as a pass-through from single-mode waveguides to wide intensity distribution required by the photonic crystal polarizer (and vice-versa, from wide intensity distribution to single-mode waveguides).

The input linear waveguide is terminated with a parabolic tapered waveguide in order to reduce diffraction when coupling light into the crystal. This is achieved through extending the area of interaction, which minimizes the angular distribution of the incident k-vector. A large angular distribution of the k-vectors leads to higher optical losses. This is due to the fact that more light is incident on the structure walls below the critical angle for total internal reflection. The effect is significant in this case as the low refractive index contrast determines a large angle. Parabolic tapered waveguides are present for the output

as well, but with reverse functionality. Their purpose is to collect an couple light to the output waveguides with minimal losses. There are visible differences between the parabolic tapered waveguides for the TM and TE outputs. These differences arise from the specific parameters for each case, such as the traverse distribution of intensity and angular distribution of k-vectors. Using large optical components means that light propagates through more material. Further experimental investigations are required for optimizing the balance between absorption and losses from evanescent waves due to the angle of incidence on the structure walls.

As light passes through the photonic crystal, the intensity distribution widens considerably (see fig. 5.b)) along with the k-vectors angular distribution. In order to compensate these effects, we employ a MMI. This component is based on the excitation of multiple modes in a waveguide and the interference between them. It functions similarly with a resonant cavity. This effect is significant for waveguides considerably larger than the wavelength. The width should be equal to an integer number of half-wavelengths, in order to act as a resonant cavity. In this case, the width of the MMI is 2.34 μm ($6 \cdot \lambda/2$). MMI are usually used with linear waveguide inputs that are situated symmetrically to the longitudinal axis. In such case an effect called "self-imaging" occurs, which results in near 100% coupling over lengths varying from microns to tens of microns. In the discussed case, however, the input is dictated by the photonic crystal and the input parabolic tapered waveguide. This design determines a transverse intensity profile that is not symmetric in relation to the longitudinal axis.

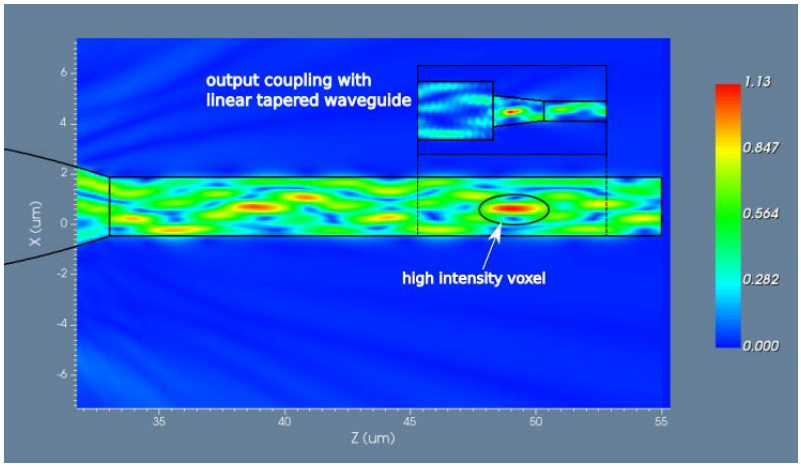

Fig. 4: Formation of the high intensity voxel in the MMI.

Quickest approach to design such a device is to first set the desired width (integer number of half-wavelengths) and inputs. Its length is arbitrarily chosen. However, we must consider that the device should be long enough for the excitation of multiple modes and interference between them to occur. When the geometry is set, a FDTD simulation is started. If the length of the device was enough, then the propagating light should present hot-spots where all excited modes interfere constructively in a defined area/volume. If there are no hot-spots present, then the length of the MMI is not enough and another FDTD simulation is required. It is worth mentioning that simulating very long MMI is not necessary, as the propagation through such a device has a periodic behavior. In other words, the simulated intensity distribution is going to repeat at specific spatial intervals, determined by the geometry of the device.

Although the imaging efficiency is not comparable to a symmetric input, the MMI utilized in the device generates a high intensity voxel. The term "voxel" is used to describe a prolate volume where intensity is highest. It is usually used to describe the focal point of a lens where the intensity is over a specific threshold. The voxel formation and position can be observed in figure 4.

The voxel is situated at 15 μm from the entry point of the MMI. At this position we construct the coupling to the output waveguide, which is mediated by a 2 μm short linear tapered waveguide to fine-tune the coupling efficiency.

The light source is continuous wave with λ=780 nm with a Gaussian transverse intensity profile. Its width (full width at $1/e^2$) of ~1.1 μm is centered on the input linear waveguide. The effective refractive index is locally calculated using the design parameters. The software package offers the possibility of calculating propagation modes for the refractive index distribution where the light source is positioned and calculate the effective refractive index for each resulted mode. The amplitude is the default value of 1 V/m and can be considered arbitrary, as there are no parameters that vary with the input amplitude in the simulated device, i.e. the refractive index has real values.

In our design, TE modes are reflected from the photonic crystal and coupled into an output waveguide (figure 5.a)). The TM modes are transmitted through the photonic crystal and coupled into the MMI and then to the TM output (figure 5.b)). Simulations are shown in figure 5.a) (TE modes) and 5.b) (TM modes). In the TE case, it can be observed that there is no light transmitted through the crystal. The output coupling is affected by interference with the input light and by the diffraction due to reflection on the periodically structured side of the photonic crystal. In the TM case, light propagates through the crystal and is efficiently coupled to the output waveguide. The necessity of a parabolic tapered waveguide can be observed in figure 5.b). The larger area of interaction at the

input of the crystal, and the TM photonic band structure (figure 3) determined a largely distributed intensity distribution with respect to X axis, as well as a small offset downwards on the X axis (figure 5.b)). The length of the parabolic tapered waveguide was optimized to guide as much light as possible to the MMI, while avoiding small angles of incidence. This results in more light going through total internal reflection, therefore minimizing optical losses through evanescent waves.

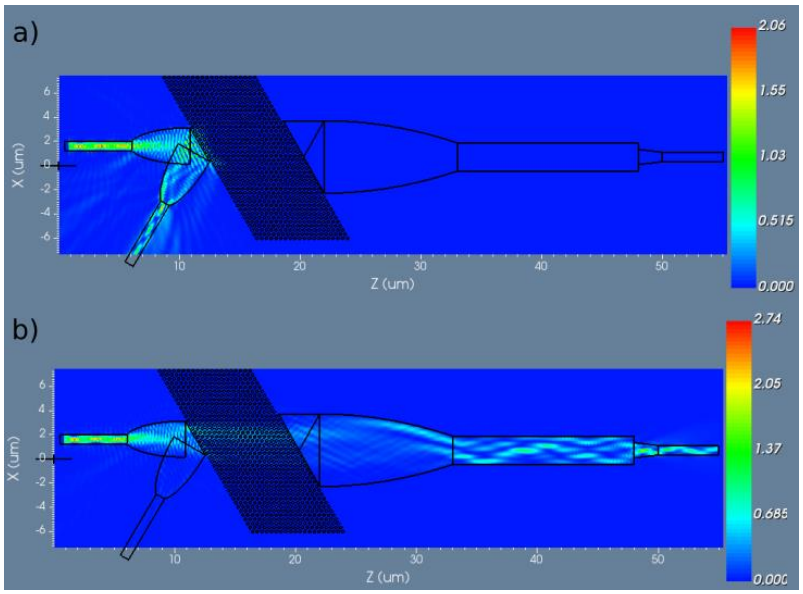

Fig. 5: Simulated intensity distribution using an input source with a Gaussian transverse profile and a maximum amplitude of 1 V/m : a) for TE modes, b) for TM modes.

As previously mentioned, the functionality of the MMI should not be affected by the input parameters of the PBS itself. The transverse distribution of intensity at the entrance of the MMI is determined by the photonic crystal and the parabolic tapered waveguide. Due to the large interaction area, the behavior of the MMI does not change with respect to input parameters.

3. Experimental results for IP-L based photonic crystals

The device is fabricated using TPP-DLW (Nanoscribe Photonic Professional). This method, as well as materials, offer several advantages such as resolution beyond the diffraction limit, straightforward implementation, reduced costs and time-efficiency. The simplest procedure consists of drop casting liquid

photoresist on the substrate, laser exposure and development. The development of the sample is done through immersion in PGMEA (propylene glycol methyl ether acetate) for 10-15 minutes and then leaving the sample to dry. The method and materials offer an option for cheap and fast prototyping of photonic devices and circuits. Moreover, the method can be complementary to electron lithography of Silicon-on-Insulator (SOI) devices as a method of chip interconnection through photonic wire bonds [20].

The fabrication method is described in figure 6. The polymeric photoresist is irradiated using 120 fs laser pulses with a frequency of 80 MHz and a central wavelength of λ=780 ± 10 nm. The beam was focused using a 100x oil-immersed microscope objective with a numerical aperture NA=1.3. For the parametrization, structures were written on a 170 μm thick glass substrate. To increase the probability of two photon absorption, high local intensities are required. Laser parameters are set so that only the top of the Gaussian intensity distribution exceeds the threshold value for polymerization to take place. This generates spatial features under the diffraction limit.

We chose the photonic crystal for parametrization since it has the smallest geometric features. Fabricating this component validates our method and materials. The parameters taken into consideration were: laser power, cylinder height and distance between cylinders. Parameters for a fixed distance between cylinders of 700 nm can be observed in table 1. It is worth noting that cylinder height varies with the focus position as well as the laser power. For a laser power of 40 mW, the voxel has a height of ~2 μm and a diameter of less than 1 μm. All cylinders are started from 0.5 μm inside the glass substrate, to ensure the adherence of the polymer. Parametrization is designed as a power vs cylinder height matrix.

Experimental results for the power vs. height sample can be observed in figure 7 (top-down Scanning Electron Microscope (SEM) image). Results indicate that for aspect ratios lower than 1:5 (diameter : height), cylinders weld together. This happens because the structure is flexible and may present surface electrostatic charges before developing and drying the sample. Cylinder welding also strongly depends on distance between them. This effect could also be induced by the development stage, especially pulling the sample from the developer and drying, due to surface tension of the liquid.

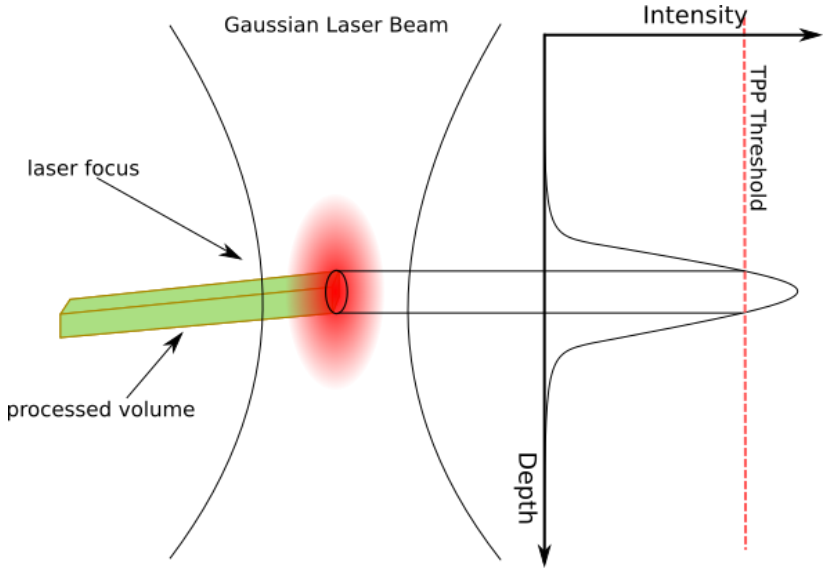

Fig. 6: TPP-DLW principle of operation: only the top of the Gaussian intensity distribution exceed the polymerization threshold, resulting in sub-wavelength spatial features.

Table 1

Processing parameters for a primitive cell vector of 700 nm

Laser power (mW)	25	30	35	40
Cylinder height (μm)	0.5	2.5	4.5	6.5

Positioning accuracy of the laser beam is excellent throughout the parametrization map (figure 7). A close-up of the crystal constructed with a laser power of 35 mW and height 0.5 μm is presented in figure 8. It can be observed that cylinders are identically constructed throughout the crystal, but their shape is rounded towards the end. This happens due to the shape of the voxel. The resulted shape will affect the photonic band structure of the device. The second image (8.b)) is taken at a 30 deg angle. Cylinder height is ~1 μm with a diameter of ~0.3 μm.

The diameter of the cylinders increase with ~100 nm for each 5 mW of laser power. The smallest geometric features are obtained with a laser power of 30 mW and the positioning remains excellent even at the target distance between cylinders of ~0.4 μm, as it can be seen in figure 9.a). However, the structure does

not function as a photonic crystal due to the very low cylinder height. This might be due to not bringing the voxel to an appropriate height, resulting in most of the power being focused inside the substrate. It is worth noting that all cylinders are started from 0.5 μm inside the glass substrate.

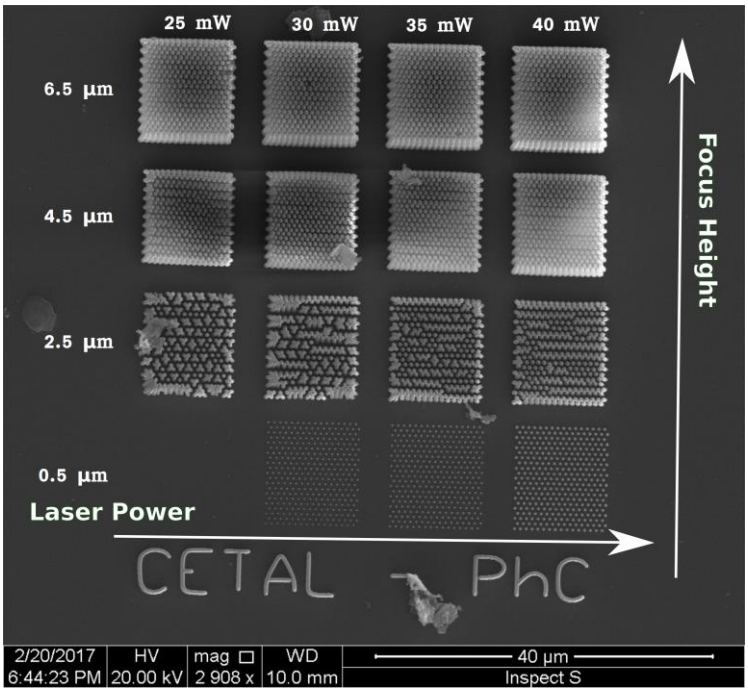

Fig. 7: Parametrization map, laser power vs. cylinder height for a primitive cell vector of 700 nm.

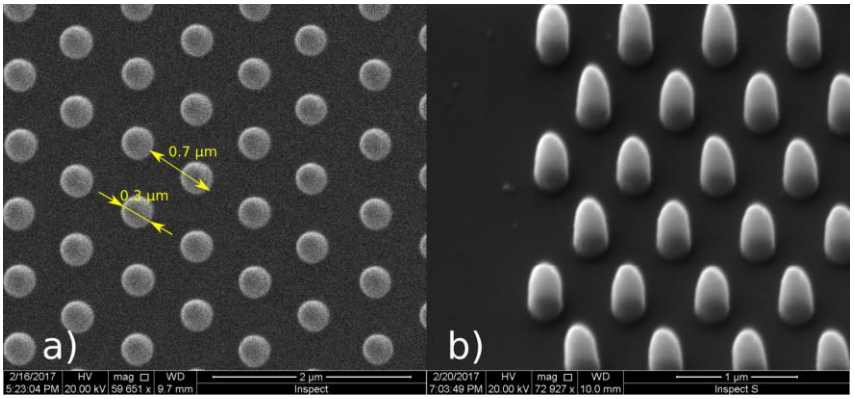

Fig. 8: Close-up of the crystal: a) for a laser power of 35 mW and a height of 1 μm, b) 30 deg angle of the same structure

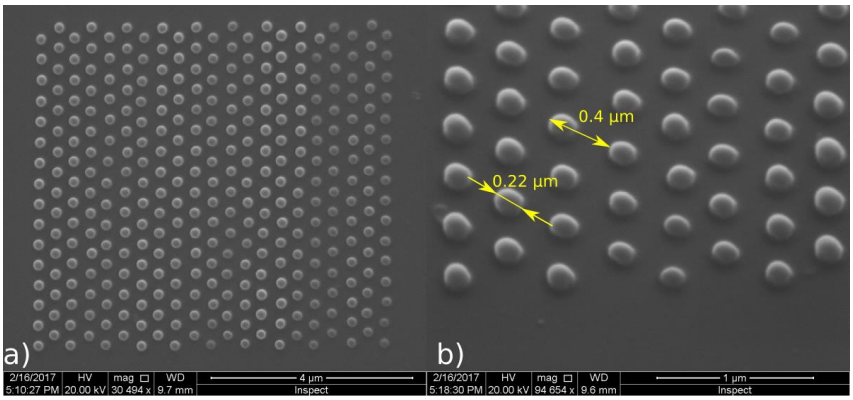

Fig. 9: Experimental results: ~0.22 µm cylinders, with a distance of ~0.4 µm between them, for a laser power of 30 mW: a) top-down view, b) 30 deg angle.

Cylinders were visibly shrinking in real time during the image optimization phase, when the electron beam was focused on a single cylinder. This could be another possible reason for the lack of height. A 14 nm thin gold film was deposited on the samples before scanning in order to avoid surface charge accumulation that would hinder the SEM image acquisition.

4. Conclusions

We have designed a novel photonic device that acts as a narrow-band polarization beam splitter, designed to function for a wavelength of λ=780 nm. The device is comprised of various photonic components that include parabolic tapered waveguides, linear waveguides and a multimode interference coupler, which contribute to the efficiency of the primary component which is a 2D photonic crystal of polymeric photoresist cylinders in air. The targeted materials and fabrication method are intended to be an option for fast and cheap prototyping of complex photonic structures. Design steps and simulation results are presented and discussed. Experimental results indicate that photonic crystals with features down to ~200 nm and primitive cell vectors of ~400 nm can be fabricated through two-photon polymerization direct laser writing, but further investigations are required to determine optimal parameters for cylinder height and structural integrity. Possible applications of such a device are varied, among which polarization filters, optical measurements for lab-on-a-chip devices, photonic circuits for quantum key distribution and on-chip optical information processing can be mentioned.

R E F E R E N C E S

[1] *J. Kim, H. K. Kim et. al*., The Fabrication of a Photonic Crystal Fiber and Measurement of its Propoerties, Journal of the Optical Society of Korea, vol. 7, no. 2, pp. 79-83, (2003);
[2] *Y. Ohtera et. al.,* Ge/SiO2 Photonic Crystal Multichannel Wavelength Filters for Short Wave Infrared Wavelengths, Japanese Journal of Applied Physics, vol. 46, no. 4A, pp. 1511-1515, (2007);
[3] *E. Schonbrun et. al.,* Polarization beam splitter based on a photonic crystal heterostructure, Optics Letters, vol. 31, no. 21, pp. 3104-3106, (2006);
[4] *J. She et. al.,* High-efficiency polarization beam splitters based on a two-dimensional polymer photonic crystal, Journal of Optics A: Pure and Applied Optics, vol. 8, pp. 345-349, (2006);
[5] *W. Zheng et. al.,* Integration of a photonic crystal polarization beam splitter and waveguide bend, Optics Express, vol. 17, no. 10, pp. 8657-8668, (2009);
[6] *V. Zabelin et. al.,* Self-collimating photonic crystal polarization beam splitter, Optics Letters, vol. 32, no. 5, pp. 530-532, (2007);
[7] *Y. C. Shi*, A Compact Polarization Beam Splitter Based on a Multimode Photonic Crystal Waveguide with an Internal Photonic Crystal Sectrion, Progress in Electromagnetics Research, vol. 103, pp. 393-401, (2010);
[8] *S. Tanzili et. al.,* On the genesis and evolution of Integrated Quantum Optics, Laser & Photonics Reviews, vol. 6, no. 1, pp 115-143, (2012);
[9] *C. Jamois et. al*., Silicon-based two-dimensional photonic crystal waveguides, Photonics and Nanosctructures – Fundamentals and Applications, vol. 1, no. 1, pp. 1-13, (2003);
[10] *M. Belotti et. al*., All-optical switching in 2D silicon photonic crystals with low loss waveguides and optical cavities, Optics Express, vol. 16, no. 15, pp. 11624-11636, (2008);
[11] *K. Inoshita et. al.,* Fabrication of GaInAsP/InP Photonic Crystal Lasers by ICP Etching and Control of Resonant Mode in Point and Line Composite Defects, IEEE Journal of Selected Topics in Quantum Electronics, vol. 9, no. 5, pp. 1347-1354, (2003);
[12] *D. F. Sievenpiper et. al*., 3D Wire Mesh Photonic Crystals, Physical Review Letters, vol. 76, no. 14, pp. 2480-2483, (1996);
[13] *C. McGuinness et. al.,* Woodpile Structure Fabrication for Photonic Crystal Laser Acceleration, Advanced Accelerator Concepts 2008 Proceedings, SLAC-PUB-13414, (2008);
[14] *Y. H. Ye et. al.,* Self-assembly of three-dimensional photonic-crystals with air-core line defects, Journal of Materials Chemistry, no. 12, pp. 3637-3639, (2002);
[15] *M. Deubel et. al*., 3D-2D-3D photonic crystal heterostructures fabricated by direct laser writing, Optics Letters, vol. 31, no. 6, pp. 805-807, (2006);
[16] *J. Haberko et. al*., Fabrication of mesoscale polymeric templates for three-dimensional disordered photonic materials, Optics Express, vol. 21, no. 1, pp. 1057-1065, (2013);
[17] *Y. F. Chau et. al.,* Evolution of the complete photonic bandgap of two-dimensional photonic crystal, Optics Express, vol. 19, no. 6, pp. 4862-4867, (2011);
[18] *S. G. Johnson et. al*., Guided modes in photonic crystal slabs, Physical Review B, vol. 60, no. 8, pp. 5751-5758, (1999);
[19] *Y. Kalra and R. K. Sinha*, Photonic band gap engineering in 2D photonic crystals, Pramana – journal of physics, vol. 67, no. 6, pp. 1155-1164, (2006);
[20] *N. Lindenmann et. al.,* Photonic wire bonding: a novel concept for chip-scale interconnects, Optics Express, vol. 20, no. 16, pp. 17667-17677, (2012);